

Coherent Holocene expansion of a tropical Andean and African glacier

Anthony C. Vickers

A thesis

submitted to the Faculty of

the department of Earth and Environmental Science

in partial fulfillment

of the requirements for the degree of

Masters of Science

Boston College

Morrissey College of Arts and Sciences

Graduate School

August 2018

Coherent Holocene expansion of a tropical Andean and African glaciers

Anthony C. Vickers

Advisor: Jeremy D. Shakun, PhD.

Abstract

Glaciers in the tropics have undergone significant retreat in the past several decades, but the magnitude of this retreat in the long-term context of the Holocene has mostly been qualitatively assessed. This study produces a quantitative reconstruction of Holocene glacier extent relative to today from the Quelccaya Ice Cap, Peru, and the Rwenzori Mountains of east Africa. I use measurements of *in situ* ^{14}C and ^{10}Be from bedrock that was recently exposed by glacier retreat to constrain possible bedrock exposure and erosion histories at each site. The results are strikingly similar in both areas, and suggest that ice was generally smaller than today during the first half of the Holocene and larger than today for most, if not all, of the last several millennia. These findings give evidence toward a coherent Holocene expansion of glaciers across the tropics, and suggest that recent retreat is unusual in a multi-millennial context.

Table of Contents

Contents

List of Tables	v
List of Figures	vi
Introduction	1
1.0 Background	2
1.1. Modern Climate.....	2
1.2. Tropical Glacier Dynamics	4
1.3. Study Sites.....	5
1.4. The ^{14}C - ^{10}Be chronometer.....	6
2.0. Methods	7
3.0. Results	8
4.0. Discussion	10
Acknowledgements	12
Figures	13
References	16
Supplementary Material	20
Supplemental References	31

List of Tables

Supplementary Table S1. ^{10}Be and ^{14}C sample data.

Supplementary Table S2. ^{10}Be sample data details.

Supplementary Table S3. ^{14}C sample data details.

Supplementary Table S4. ^{10}Be blank data.

List of Figures

Figure 1. Locations of samples of recently exposed bedrock

Figure 2. ^{14}C and ^{10}Be concentrations in bedrock samples from the Quelccaya Ice Cap and the Rwenzori Mountains.

Figure 3. Inferred tropical glacier histories compared to paleoclimate records.

Supplementary Figure S1. Aerial photo of Weismann Peak, Rwenzori Mountains, from 1937.

Supplementary Figure S2. Photographs of recently deglaciated bedrock samples from the Quelccaya Ice Cap and Rwenzori Mountains.

Supplementary Figure S3. Graphical depiction of all modeled Holocene exposure scenarios.

Supplementary Figure S4. The median age of exposure and cumulative exposure duration for each modeled exposure scenario.

Supplementary Figure S5. Exposure scenarios that yield ^{14}C and ^{10}B concentrations within 3σ of the measured samples for the Quelccaya Ice Cap and Rwenzori Mountains samples.

Supplementary Figure S6: Erosion rates for viable model scenarios for the Quelccaya Ice Cap and the Rwenzori Mountains.

Introduction

Anthropogenic greenhouse gas emissions have driven a rise in global mean temperature and caused global variations in precipitation over the past century (IPCC, 2013). As a result, glaciers around the world have exhibited marked retreat (Marzeion et al., 2014). However, it is generally unclear how current glacier extents compare to their long-term average over the Holocene and how their lengths varied during this interval (Solomina et al., 2015). Moreover, the short instrumental record is insufficient to determine glacier sensitivities to changes in climate. Such information is important for placing current retreat in a geologic context and projecting future glacier changes, which will affect freshwater resources in many areas (Vuille et al. 2008) and global sea level (IPCC, 2013).

The Holocene history of tropical glaciers, in particular, is poorly constrained. Existing records of glacier length are typically qualitative or discontinuous, and biased toward intervals of expanded ice cover (Solomina et al., 2015). Consequently, these records have produced contrasting views on the evolution of tropical glaciers over the Holocene. For instance, clastic sediment fluxes to proglacial lakes in the Andes suggest reduced ice cover during the early Holocene followed by a neoglaciation in the late Holocene (Rodbell et al., 2009), which parallels the general expansion of Northern Hemisphere glaciers due to declining boreal summer insolation (Solomina et al., 2015). Alternatively, moraine ages in the tropical Andes suggest an overall decline in glacier extent through the Holocene (Jomelli et al., 2014; Jomelli et al., 2011), similar to the contraction of Southern Hemisphere glaciers presumably related to rising austral summer insolation (Putnam et al., 2012).

To generate a more complete and quantitative Holocene record of tropical glaciation, I apply the *in situ* ^{14}C - ^{10}Be chronometer to bedrock (Goehring et al. 2011) at the margin of the Quelccaya Ice Cap, Peru and a recently deglaciated site in the Rwenzori Mountains of east Africa. The use of multiple cosmogenic nuclides enables an estimate of the cumulative amount of time, and broadly when, the glaciers were larger or smaller than today, informing our understanding of how anomalous current glacier retreat may be in a Holocene context as well as what drove their long-term trends over this time.

1.0 Background

1.1. Modern Climate

Studying how present day tropical glaciers respond to changes in climate is paramount to understanding how they have changed in the past and how they will change in the future. In terms of glacier response, the tropics can be subdivided into the inner and outer tropics. Both zones have little seasonality in terms of temperature. Their main differentiation is derived from their position relative to the annual migration of the Intertropical Convergence Zone (ITCZ). The ITCZ is globally located around the equator, where the Northern Hemispheric northeast trade winds meet the Southern Hemispheric south east trade winds. Where the two wind regimes meet and converge the air masses begin to rise due to solar heating, forming the upwelling portion of the Hadley Cells. Owing to this convection process, the ITCZ is marked by cloud formation and precipitation. Its location shifts northward and southward throughout the year depending on the zenith position of the sun. The shift is most dramatic over continents due to their low specific heat compared to the oceans. Thus in boreal summer, the ITCZ is located more north, while during austral summer, the ITCZ is located south of the equator.

Broadly, the inner tropics are defined by having a wet climate year round with peak precipitation happening twice a year corresponding with the oscillation of the ITCZ overhead, while the outer tropics have both a wet and a dry season, with one peak in precipitation associated with the passage of the ITCZ.

The amount of precipitation on tropical continents is also influenced by the strength of monsoons and by teleconnections linked to El Niño-Southern Oscillation (ENSO) variability. During El Niño (La Niña) years, sea surface temperature (SST) in the eastern equatorial pacific increases (decreases), which promotes convection (subsidence) on the western flank of South America. The convection (subsidence) weakens (strengthens) upper tropospheric easterlies that are responsible for bringing moisture laden air across the Amazon Basin, which in turn decreases (increases) the amount of precipitation that the Cordilleras and the Altiplano receive. However, it should be noted that the complete mechanism for the precipitation patterns is not fully known and the above explanation is one of many (Gareaud et al., 2009). In addition, Casimiro et al. (2013) found that the multivariate ENSO index only correlates with ~15% of annual variations in precipitation in the southern Andes.

The South American Summer Monsoon occurs during the austral summer (December, January, February) and is responsible for over 50% of the annual precipitation in the outer tropics (Silva and Kousky, 2012). During the summer months, the air temperature over the land is warmer than over the Atlantic Ocean, which causes lower pressures over land and higher pressures over the ocean. This pressure gradient facilitates moist air originating in the Atlantic Ocean to move over South America and deliver monsoon precipitation. The unique topographical characteristics of South

America dictate the path and form of the monsoon. The Andes in the west provide a barrier for the westward-flowing moisture-laden air and deflect them south over western Brazil (Silva and Kousky, 2012).

The East African Monsoon is associated with the seasonal shift of the ITCZ, which is associated with peaks in precipitation. One peak occurs from March to May and the second peak occurs from October to December. Between the two peaks, east equatorial Africa experiences its pronounced dry seasons. In addition, positive ENSO events are typically associated with high precipitation in the region. SST in the Indian Ocean and the Atlantic Ocean have also been correlated with precipitation variations here (Nicholson, 1996).

1.2. Tropical Glacier Dynamics

There are several key differences between tropical glaciers and their mid to high-latitude counterparts. Owing to the warm temperatures of the tropics, glaciers are restricted to high elevations. The position of the glacier, and more specifically the equilibrium line altitude (ELA), which is the transition zone between accumulation (glacier growth) and ablation (glacier recession), is generally dictated by the 0°C isotherm, with accumulation above and ablation below. However, in the wet inner tropics the ELA can be found below this isotherm, and in the wet-dry outer tropics the ELA may lie above it. The lack of temperature seasonality in both the inner and outer tropics permits constant, year-round removal of snow and ice (ablation) from glaciers. In the inner tropics, tropical glaciers experience accumulation throughout the year with two peaks in precipitation, while glaciers in the outer tropics experience accumulation only during the wet season. Thus, in the wet inner tropics, glaciers respond most strongly to

changes in temperature, whereas glaciers in the dry outer tropics are more sensitive to changes in precipitation (Kaser, 2001; Rodbell et al, 2009). In addition, glacier responses to climate are dependent on the aspect and the gradient of the slope where the glacier resides. A glacier facing a direction that is unobstructed from precipitation-laden air masses or more sheltered from direct sunlight will be less sensitive than a glacier that is shielded from moisture or sunlight. Glaciers located on steeply sloping terrain similarly retreat less due to changes in climate than those located on gently sloping terrain.

1.3. Study Sites

The Quelccaya Ice Cap in the Peruvian Andes (13.9°S, 70.8°W, 5740 m) is the largest tropical ice mass in the world, covering 44 km² (Figure 1A). It is particularly sensitive to changes in climate owing to its relatively low relief and dome shape, which enables a small change in temperature to drive a potentially large change in the ablation area of the ice cap, and thus of its marginal position (Mark et al. 2002). Indeed, Quelccaya's outlet glaciers have been retreating in recent decades in response to increasing air temperature (Brecher and Thompson, 1993; Thompson, 2000; Thompson et al. 2011; Rabatel et al. 2013). The current catalog of Holocene ice margin constraints provides patchy but useful information. Radiocarbon dating suggests that the ice retreated to near or within its late Holocene extent by 11.6 ka during the last deglaciation (Kelly et al., 2012), and was as small or smaller than today from ≥ 7 to 5.2 ka (Buffen et al., 2009). Thereafter, 5-kyr old in-place plant material exposed by recent retreat of the ice cap suggests that the ice was more extensive than today, because the material would have decomposed if it had been uncovered previously, with late Holocene advances culminating at ~ 2.7 ka and ~ 0.5 ka (Mark et al., 2002; Stroup et al., 2014, 2015).

The Rwenzori Mountains of Uganda (0.3°N, 29.9°E, highest elevation 5109 m) feature the most extensive system of glaciers on the African continent, though these have also exhibited substantial retreat over the past century and <1 km² of ice now remains (Hastenrath and Kruss, 1992; Kaser and Osmaston, 2002; Thompson et al., 2002; Taylor et al., 2006) (Figure 1B). The Holocene glacial history is poorly constrained, with one glacial advance ~10 ka and another ~0.3 ka (Kaser and Osmaston, 2002). The youngest deglacial moraine down valley from the samples analyzed in this study has a mean ¹⁰Be age of 11.2 ± 0.3 ka (n=4) (Margaret Jackson, personal communication, 2018).

1.4. The ¹⁴C-¹⁰Be chronometer

Concentrations of ¹⁴C and ¹⁰Be in proglacial bedrock, and the ratio between them, are a function of the history of ice cover and erosion at the site and can thus be used to reconstruct these variables (Goehring et al., 2011). During intervals of reduced ice extent, exposure to cosmic radiation produces ¹⁴C and ¹⁰Be in the bedrock at a ratio of ~3.5, and the nuclide concentrations build up in proportion to the duration of exposure. When ice advances over the site, production stops and the nuclides decay. However, whereas ¹⁰Be decay is negligible on Holocene time scales ($t_{1/2} = 1.39$ Myr), ¹⁴C concentrations can decline significantly during burial owing to its relatively short half-life (5730 years), which decreases the ¹⁴C/¹⁰Be ratio through time. Additionally, glacial erosion reduces the concentrations of both nuclides by scraping off the rock surface, where concentrations are highest in the top couple of meters of the rock column due to the exponential decline of nuclide production rates with depth. Thus, the Holocene history of ice extent relative to today can be constrained by measuring ¹⁴C and ¹⁰Be concentrations in a series of recently exposed bedrock samples taken along the current ice

margin, which would have experienced the same exposure history. This approach requires that the bedrock surface was sufficiently eroded during the last glaciation to remove nuclides produced during episodes of exposure prior to the Holocene, and that the bedrock was only covered by ice in the past (e.g., not till). These assumptions can be assessed based on the coherency of $^{14}\text{C}/^{10}\text{Be}$ ratios in the samples, since the samples would be unlikely to contain the same amount of pre-Holocene nuclide inheritance or have experienced the same history of sediment cover through time.

2.0. Methods

Five bedrock samples were collected along the western edge of the Quelccaya Ice Cap, close to the 5 ka plant remains dated by Buffen et al. (2009) (Figure 1A). All samples were within meters of the ice margin at the time of sampling (2003). Two additional bedrock samples were collected 3 km down valley from this site to better constrain the timing of the last deglaciation and provide a maximum-limiting age for initial Holocene exposure. Three bedrock samples were also taken from a headwall high on Weismann's Peak in the Rwenzori Mountains, which was deglaciated within the past 70 years as evidenced by historical photography (Supplementary Figure S1). All samples were from smooth bedrock surfaces with no nearby sediment cover (Supplementary Figure S2).

We measured ^{14}C and ^{10}Be concentrations in all samples of recently deglaciated bedrock, and only ^{10}Be in the two samples down valley from the Quelccaya Ice Cap. Sample processing and chemistry were conducted at Purdue University. Quartz was isolated using standard protocols (Kohl and Nishizumi, 1992). ^{14}C was extracted following the methods of Lifton et al. (2001) and Pigati (2004), and ^{10}Be was extracted

according to the methods used by Lamont-Doherty Earth Observatory (<http://www.ldeo.columbia.edu/tcn/>). Isotopic ratios were measured at Lawrence Livermore Center for Accelerator Mass Spectrometry (^{10}Be) and Woods Hole National Ocean Sciences Accelerator Mass Spectrometry facility (^{14}C). More detailed descriptions of sample processing are provided in the supplementary material.

Measured nuclide concentrations may be consistent with a number of Holocene glacier histories, which were evaluated through 100,000 Monte Carlo simulations that explore a wide range of exposure scenarios (Supplementary Figure S3). Each scenario uses the same exposure history for each sample and a range of erosion rates. The simulation models nuclide production in a column of bedrock for each sample site via exposure when ice-free, and nuclide loss via erosion and decay when ice-covered. Only histories with initial exposure at or after 11.6 ka are considered, based on evidence mentioned above that ice had not retreated near the sampling sites before this time during the last deglaciation. Scenarios that yield bedrock surface nuclide concentrations in agreement with measured concentrations of both nuclides in all samples are considered plausible. Production rates are taken from the CRONUS online calculator v3 (Balco et al., 2008) using the LSDn scaling scheme (Lifton et al., 2014).

3.0. Results

Measured ^{14}C and ^{10}Be concentrations and ratios for the recently deglaciated Quelccaya and Rwenzori samples are, in general, strikingly similar, suggesting similar glacier histories at both sites (Supplementary Table S1). The highest concentration ^{10}Be samples at both locations record at least ~5 kyr of exposure, while $^{14}\text{C}/^{10}\text{Be}$ ratios are low (~1/3 the production ratio), implying ~6-8 kyr of burial (Figure 2). The Rwenzori

samples all have relatively high nuclide concentrations, consistent with minimal erosion, while the Quelccaya samples exhibit a larger range of concentrations, suggesting that some have been more deeply eroded than others. The $^{14}\text{C}/^{10}\text{Be}$ ratios of all samples are similar (0.83 ± 0.03 to 1.07 ± 0.04 for the Rwenzori samples, 0.84 ± 0.04 to 1.21 ± 0.05 for Quelccaya samples; 1σ uncertainties), implying concordant burial histories, except sample Q-81 (0.35 ± 0.02), which has a substantially higher ^{10}Be concentration than any other sample and records 24 kyr of total history; this sample is therefore considered contaminated by pre-Holocene inheritance and excluded. The two bedrock samples from a few kilometers down valley of the Quelccaya ice margin have ^{10}Be ages of 11.0 ka, confirming the presumption that initial Holocene exposure did not occur until after this time (Supplementary Table S1).

Monte Carlo simulations suggest that only a small subset of exposure scenarios can explain the measured nuclide concentrations at both sites (0.01% of simulations), and all are primarily dominated by exposure in the early Holocene and burial in the late Holocene (Figure 3). The data tightly constrain the glacial histories because the highest concentration ^{10}Be samples require at least 5 kyr of exposure, while the low $^{14}\text{C}/^{10}\text{Be}$ ratios imply that the samples were radioactively decaying under ice cover for millennia following this exposure; in fact, more than a few centuries of exposure after 5 ka would elevate $^{14}\text{C}/^{10}\text{Be}$ ratios above their measured values. Inferred erosion rates are 1-50 mm/kyr for the Quelccaya samples and 0-5 mm/kyr for the Rwenzori samples, similar to rates estimated for the Rhone Glacier, Switzerland, also based on proglacial $^{14}\text{C}-^{10}\text{Be}$ measurements (Goehring et al., 2011).

4.0. Discussion

A large majority of the simulated histories that agree with the sample measurements show a general pattern of more early Holocene exposure followed by more dominant mid to late Holocene burial. This pattern at Quelccaya aligns well with prior studies of Andean glacier variations (Rodbell et al., 2009). For instance, records of clastic sediment fluxes to Andean glacial lakes also suggest a resurgence in glacial advance in the mid to late Holocene (Rodbell et al., 2009) (Figure 3C), and the ~5 ka age of recently exposed plant remains at Quelccaya suggest continuous ice cover since they grew (Buffen et al. 2009) (Figure 1).

What drove the long-term Holocene trend toward greater ice cover at both of these sites? The largest climate forcing over the Holocene was orbitally-driven variations in insolation. Tropical glaciers may be most sensitive to changes in mean annual, rather than seasonal, insolation since they ablate all year long (Kaser and Osmaston, 2002); however, this insolation quantity increased slightly ($\sim 1 \text{ W/m}^2$) during the Holocene, in contrast to the pattern of glacier expansion (Figure 3A). Greenhouse-gas forcing also rose during the Holocene ($\sim 0.5 \text{ W/m}^2$), which suggests that it too was not the main driver (Figure 3). Notably, while these glaciers are located at 0° and 14°S latitude, their trends parallel Northern Hemisphere glacier variations, which were typically smaller during the early Holocene Altithermal (9-5 ka) and expanded during the late Holocene Neoglaciation ($\sim 4 \text{ ka}$) in response to declining boreal summer insolation (Solomina et al., 2015). This similarity could suggest that these tropical glaciers responded to Northern Hemisphere forcings.

One possibility is that decreasing summer insolation in the Northern Hemisphere shifted the locus of tropical precipitation during the Holocene, potentially delivering more snowfall to the glaciers and driving their expansion. Indeed, numerous records suggest that the ITCZ migrated southward in South America and the South American Monsoon intensified through the Holocene (Thompson et al. 1995; Seltzer et al., 2000; Haug et al., 2001; Bird et al. 2011; Vuille et al. 2012; Kanner et al. 2013; Bernal et al. 2016) (Figure 3D), which may have increased precipitation over the southern Andes. This explanation seems unable to account for Rwenzori glacier growth, however, because precipitation throughout much of east and north Africa decreased during the mid to late Holocene as the African Humid Period ended (Tierney et al., 2010; Shanahan et al., 2015) (Figure 3F).

Alternatively, the similar pattern of glacier expansion at the two sites may point to a dominant temperature control, since it tends to covary over large scales in the tropics (Hastenrath, 2010). In addition, modern monitoring studies suggest that recent retreat of the Quelccaya Ice Cap and the Kilimanjaro Ice Field (3°S, 37°E) are largely attributable to warming (Brecher and Thompson, 1993; Thompson, 2000; Hastenrath et al 2010; Thompson et al. 2011; Rabatel et al. 2013), and the moraine and ice core record at Quelccaya similarly imply that temperature, rather than precipitation, was the main driver of ice margin fluctuations during the late Holocene (Stroup et al., 2014). A synthesis of tropical SST records suggests little overall change across the Holocene (Marcott et al., 2013) (Figure 3B), and several East African lake records similarly show comparable temperatures between the early and late Holocene (Figure 3E). It is thus unclear whether the long-term Holocene trend toward expanded ice cover found here was a result of

tropical cooling. Nonetheless, high-resolution records from east Africa and South America suggest that 20th century warming was unprecedented, or nearly so, in at least the past 1.5-2 kyr (Tierney et al., 2010; PAGES 2k Consortium, 2013), which parallels this thesis' finding that current tropical glacier extents in these areas are probably anomalous in the context of the last several millennia.

Acknowledgements

I acknowledge the help in laboratory work from Dr. Brent Goehring and help with field work and sample collection from Dr. Meredith Kelly and Margaret Jackson. This project was funded by Boston College start-up funds to Dr. Jeremy Shakun.

Figures

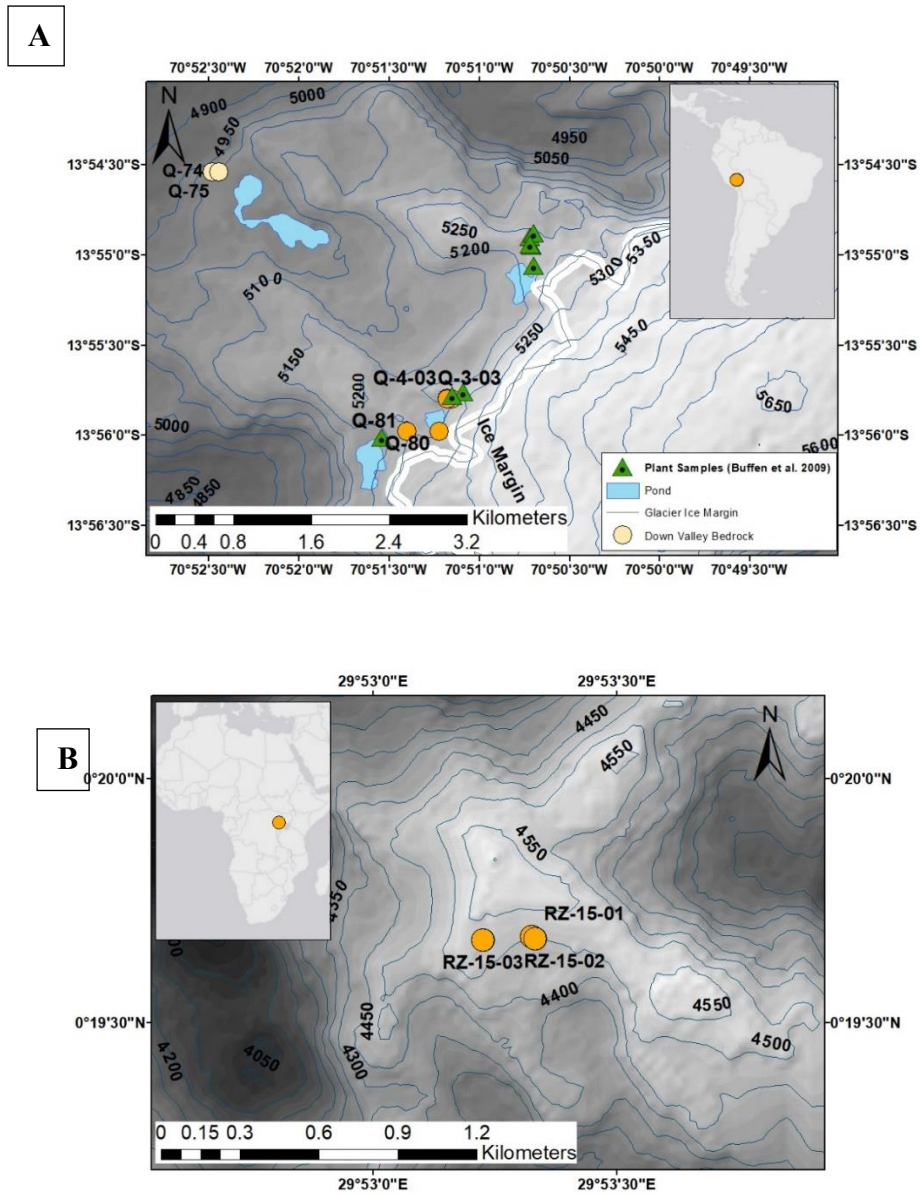


Figure 2. Locations of samples of recently exposed bedrock (dark orange circles) from **A)** the Quelccaya Ice Cap, Peru, and **B)** Weismann's Peak in the Rwenzori Mountains, Uganda. The Quelccaya Ice Cap samples were collected within meters of the retreating ice margin in 2003 (Q-2-03, Q-3-03, Q-4-03) and 2008 (Q-80, Q-81). Two additional bedrock samples down valley constrain the timing of the last deglaciation (light orange circles; Q-74, Q-75). Green triangles show recently emerged intact plant remains, which suggest ice covered this site since they grew 4700–5100 cal yr BP (Buffen et al. 2009). There is currently no glacier on Weismann's Peak, but historical photos show that ice covered the sample sites in 1937 (Supplementary Figure S1).

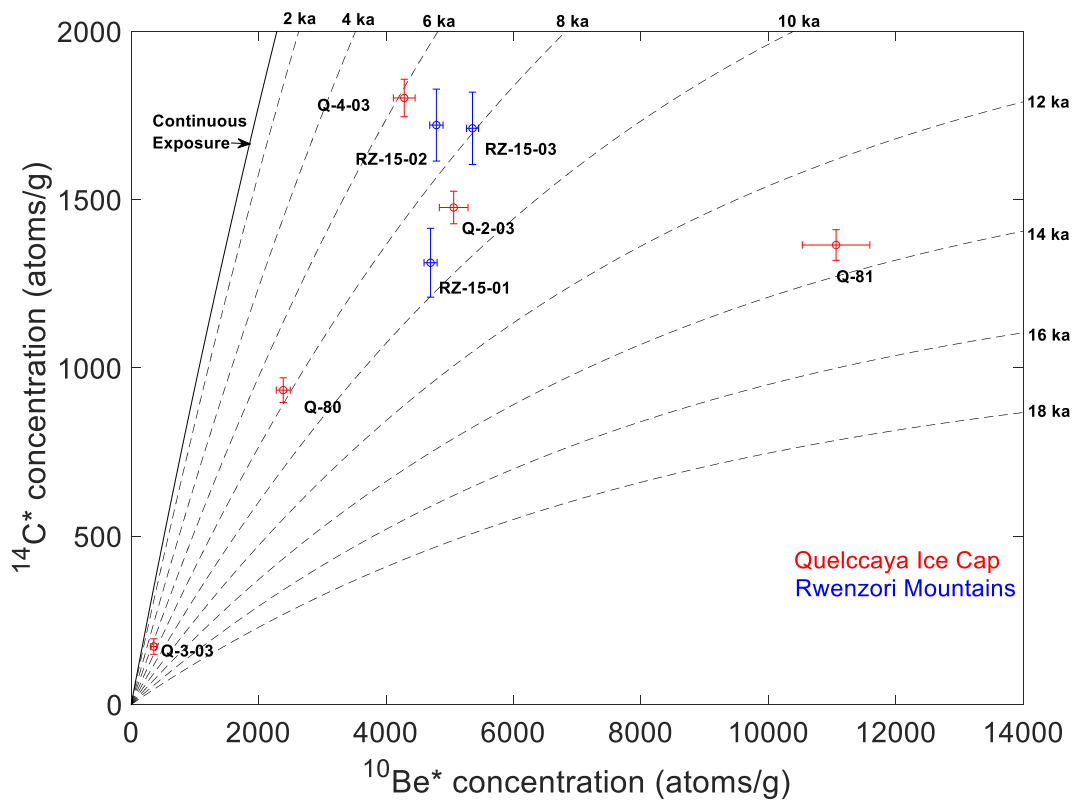


Figure 2. ^{14}C and ^{10}Be concentrations in recently exposed bedrock samples from the Quelccaya Ice Cap (red) and the Rwenzori Mountains (blue). Concentrations have been normalized by the surface production rate at each sample location, such that ^{10}Be concentrations are essentially equivalent to exposure durations in years. Error bars show 2σ measurement uncertainties. Solid black line represents the evolution of surface concentrations under continuous exposure. Dashed lines are burial isochrons, and are generated neglecting erosion.

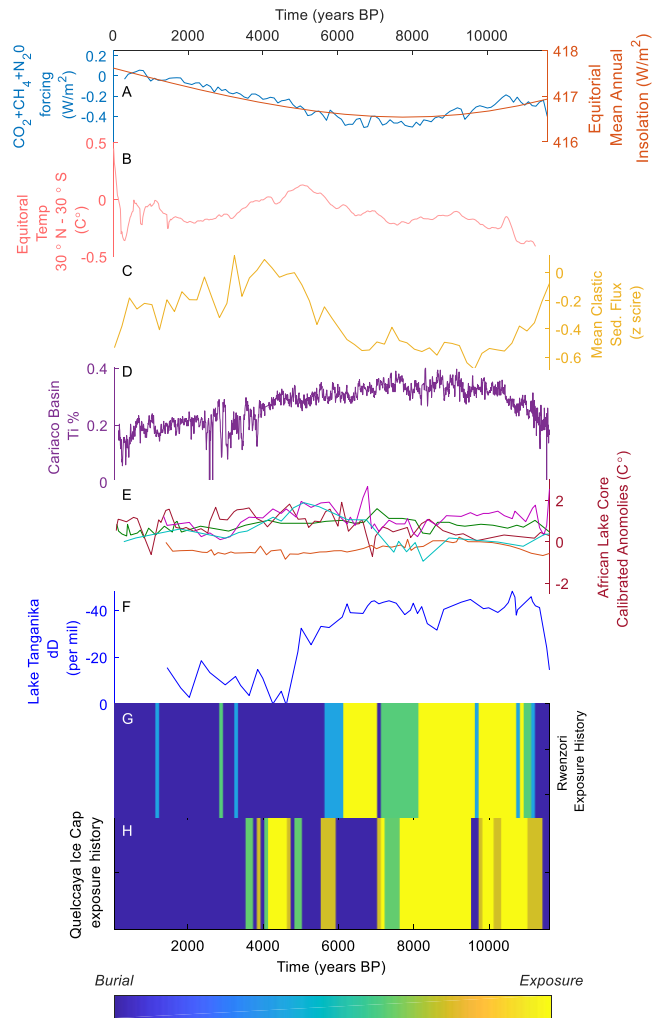


Figure 3. Inferred tropical glacier histories compared to paleoclimate records. **A)** Mean annual insolation at the equator (Laskar et al., 2004), and radiative forcing from greenhouse gases (Marcott et al., 2013). **B)** Tropical sea surface temperature stack (Marcott et al., 2013). **C)** Mean clastic sediment flux from proglacial lakes in the Andes Mountains suggesting a neoglaciation commencing ~5 ka (Rodbell et al., 2008). **D)** Cariaco Basin, Venezuela, titanium concentration, interpreted as a terrestrial runoff proxy (Haug et al., 2001). **E)** Temperature anomalies from several East African Lakes based on TEX86, including Sacred Lake (green), Rutundu (maroon), Lake Victoria (orange), Lake Tanganyika (pink), and Lake Malawi (light blue) (Powers et al., 2005; Tierney et al., 2008; Berke et al., 2012; Loomis et al., 2012, 2017). **F)** Leaf wax δD from Lake Tanganyika, which suggests a dry early Holocene followed by a mid-Holocene wetting (Tierney et al. 2008). **G, H)** Modeled exposure histories for the Rwenzori Mountain and Quelccaya Ice Cap samples analyzed in this study. Colors represent the relative proportion of successful simulations with exposure or burial during each time step. Blue indicates all scenarios modeled burial during that time period. Yellow indicates all scenarios modeled exposure during that time period.

References

- Balco, G., Stone, J. O., Lifton, N. A., & Dunai, T. J. (2008). A complete and easily accessible means of calculating surface exposure ages or erosion rates from ^{10}Be and ^{26}Al measurements. *Quaternary geochronology*, 3(3), 174-195.
- Berke, M. A., Johnson, T. C., Werne, J. P., Grice, K., Schouten, S., & Damsté, J. S. S. (2012). Molecular records of climate variability and vegetation response since the Late Pleistocene in the Lake Victoria basin, East Africa. *Quaternary Science Reviews*, 55, 59-74.
- Bernal, J. P., Cruz, F. W., Stríkis, N. M., Wang, X., Deininger, M., Catunda, M. C. A., & Auler, A. S. (2016). High-resolution Holocene South American monsoon history recorded by a speleothem from Botuverá Cave, Brazil. *Earth and Planetary Science Letters*, 450, 186-196.
- Bird, B. W., Abbott, M. B., Rodbell, D. T., & Vuille, M. (2011). Holocene tropical South American hydroclimate revealed from a decadal resolved lake sediment $\delta^{18}\text{O}$ record. *Earth and Planetary Science Letters*, 310(3-4), 192-202.
- Brecher, Henry H., and Lonnie G. Thompson. (1993). "Measurement of the retreat of Qori Kalis glacier in the tropical Andes of Peru by terrestrial photogrammetry." *Photogrammetric Engineering and Remote Sensing* 59: 1017-1017.
- Buffen, A. M., Thompson, L. G., Mosley-Thompson, E., & Huh, K. I. (2009). Recently exposed vegetation reveals Holocene changes in the extent of the Quelccaya Ice Cap, Peru. *Quaternary Research*, 72(2), 157-163.
- Garreaud, R. D., Vuille, M., Compagnucci, R., & Marengo, J. (2009). Present-day south american climate. *Palaeogeography, Palaeoclimatology, Palaeoecology*, 281(3-4), 180-195.
- Gasse, F. (2000). Hydrological changes in the African tropics since the Last Glacial Maximum. *Quaternary Science Reviews*, 19(1-5), 189-211.
- Goehring, B. M., Schaefer, J. M., Schluechter, C., Lifton, N. A., Finkel, R. C., Jull, A. T., & Alley, R. B. (2011). The Rhone Glacier was smaller than today for most of the Holocene. *Geology*, 39(7), 679-682.
- Hastenrath, S. (2010). Climatic forcing of glacier thinning on the mountains of equatorial East Africa. *International Journal of Climatology: A Journal of the Royal Meteorological Society*, 30(1), 146-152.
- Haug, G. H., Hughen, K. A., Sigman, D. M., Peterson, L. C., & Röhl, U. (2001). Southward migration of the intertropical convergence zone through the Holocene. *Science*, 293(5533), 1304-1308.
- Jomelli, V., Khodri, M., Favier, V., Brunstein, D., Ledru, M. P., Wagnon, P., & Bourles, D. L. (2011). Irregular tropical glacier retreat over the Holocene epoch driven by progressive warming. *Nature*, 474(7350), 196.

- Jomelli, V., Favier, V., Vuille, M., Braucher, R., Martin, L., Blard, P. H., ... & Bourlès, D. L. (2014). A major advance of tropical Andean glaciers during the Antarctic cold reversal. *Nature*, *513*(7517), 224.
- Kanner, L. C., Burns, S. J., Cheng, H., Edwards, R. L., & Vuille, M. (2013). High-resolution variability of the South American summer monsoon over the last seven millennia: insights from a speleothem record from the central Peruvian Andes. *Quaternary Science Reviews*, *75*, 1-10.
- Kaser, G. (2001). Glacier-climate interaction at low latitudes. *Journal of Glaciology*, *47*(157), 195-204.
- Kaser, G. and Osmaston, H. (2002). Tropical glaciers. Cambridge, etc., Cambridge University Press, xx 207 pp. map. (International Hydrology Series.) ISBN 0-521-63333-8, hardback, £75/US\$110. *Journal of Glaciology*, *49*(165), 323-323. doi:10.3189/172756503781830782
- Kelly, M. A., Lowell, T. V., Applegate, P. J., Smith, C. A., Phillips, F. M., & Hudson, A. M. (2012). Late glacial fluctuations of Quelccaya Ice Cap, southeastern Peru. *Geology*, *40*(11), 991-994.
- Lavado Casimiro, W. S., Labat, D., Ronchail, J., Espinoza, J. C., & Guyot, J. L. (2013). Trends in rainfall and temperature in the Peruvian Amazon–Andes basin over the last 40 years (1965–2007). *Hydrological Processes*, *27*(20), 2944-2957.
- Lifton, N. A., Jull, A. T., & Quade, J. (2001). A new extraction technique and production rate estimate for in situ cosmogenic ¹⁴C in quartz. *Geochimica et Cosmochimica Acta*, *65*(12), 1953-1969.
- Lifton, N., Goehring, B., Wilson, J., Kubley, T., & Caffee, M. (2015). Progress in automated extraction and purification of in situ ¹⁴C from quartz: Results from the Purdue in situ ¹⁴C laboratory. *Nuclear Instruments and Methods in Physics Research Section B: Beam Interactions with Materials and Atoms*, *361*, 381-386.
- Loomis, S. E., Russell, J. M., Ladd, B., Street-Perrott, F. A., & Damsté, J. S. S. (2012). Calibration and application of the branched GDGT temperature proxy on East African lake sediments. *Earth and Planetary Science Letters*, *357*, 277-288.
- Loomis, S. E., Russell, J. M., Verschuren, D., Morrill, C., De Cort, G., Damsté, J. S. S., & Kelly, M. A. (2017). The tropical lapse rate steepened during the Last Glacial Maximum. *Science advances*, *3*(1), e1600815.
- Marcott, S. A., Shakun, J. D., Clark, P. U., & Mix, A. C. (2013). A reconstruction of regional and global temperature for the past 11,300 years. *Science*, *339*(6124), 1198-1201.
- Mark, B. G., Seltzer, G. O., Rodbell, D. T., & Goodman, A. Y. (2002). Rates of deglaciation during the last glaciation and Holocene in the Cordillera Vilcanota-Quelccaya Ice Cap region, southeastern Peru. *Quaternary Research*, *57*(3), 287-298.

- Marzeion, B., Cogley, J. G., Richter, K., & Parkes, D. (2014). Attribution of global glacier mass loss to anthropogenic and natural causes. *Science*, *345*(6199), 919-921.
- Nicholson, S. E. (1996). A review of climate dynamics and climate variability in Eastern Africa. *The limnology, climatology and paleoclimatology of the East African lakes*, 25-56.
- Pigati, J. S., & Lifton, N. A. (2004). Geomagnetic effects on time-integrated cosmogenic nuclide production with emphasis on in situ ¹⁴C and ¹⁰Be. *Earth and Planetary Science Letters*, *226*(1-2), 193-205.
- Powers, L. A., Johnson, T. C., Werne, J. P., Castaneda, I. S., Hopmans, E. C., Sinninghe Damsté, J. S., & Schouten, S. (2005). Large temperature variability in the southern African tropics since the Last Glacial Maximum. *Geophysical Research Letters*, *32*(8).
- Putnam, A. E., Schaefer, J. M., Denton, G. H., Barrell, D. J., Finkel, R. C., Andersen, B. G., & Doughty, A. M. (2012). Regional climate control of glaciers in New Zealand and Europe during the pre-industrial Holocene. *Nature Geoscience*, *5*(9), 627.
- Rabatel, A., Francou, B., Soruco, A., Gomez, J., Cáceres, B., Ceballos, J. L., & Scheel, M. (2013). Current state of glaciers in the tropical Andes: a multi-century perspective on glacier evolution and climate change. *The Cryosphere*, *7*(1), 81-102.
- Rodbell, D. T., Smith, J. A., & Mark, B. G. (2009). Glaciation in the Andes during the Lateglacial and Holocene. *Quaternary Science Reviews*, *28*(21-22), 2165-2212.
- Seltzer, G. O., Rodbell, D. T., Baker, P. A., Fritz, S. C., Tapia, P. M., Rowe, H. D., & Dunbar, R. B. (2002). Early warming of tropical South America at the last glacial-interglacial transition. *Science*, *296*(5573), 1685-1686.
- Shanahan, T. M., McKay, N. P., Hughen, K. A., Overpeck, J. T., Otto-Bliesner, B., Heil, C. W., & Peck, J. (2015). The time-transgressive termination of the African Humid Period. *Nature Geoscience*, *8*(2), 140.
- Silva, V., & Kousky, V. E. (2012). *05 The South American Monsoon System: Climatology and Variability*. InTech.
- Solomina, O. N., Bradley, R. S., Hodgson, D. A., Ivy-Ochs, S., Jomelli, V., Mackintosh, A. N., & Young, N. E. (2015). Holocene glacier fluctuations. *Quaternary Science Reviews*, *111*, 9-34.
- Stroup, J. S., Kelly, M. A., Lowell, T. V., Applegate, P. J., & Howley, J. A. (2014). Late Holocene fluctuations of Qori Kalis outlet glacier, Quelccaya Ice Cap, Peruvian Andes. *Geology*, *42*(4), 347-350.
- Stroup, J. S., Kelly, M. A., Lowell, T. V., Applegate, P. J., & Howley, J. A. (2015). Late Holocene fluctuations of Qori Kalis outlet glacier, Quelccaya Ice Cap, Peruvian Andes. *Geology*, *43*(12), 1113-1113.

- Taylor, R. G., Rott, H., Kaser, G., Fischer, A., Cullen, N.J. (2006). "Reply to comment by T. Mölg et al. on "Recent glacial recession in the Rwenzori Mountains of East Africa due to rising air temperature"." *Geophysical Research Letters* 33(20)
- Tierney, J. E., Russell, J. M., Huang, Y., Damsté, J. S. S., Hopmans, E. C., & Cohen, A. S. (2008). Northern hemisphere controls on tropical southeast African climate during the past 60,000 years. *Science*, 322(5899), 252-255.
- Tierney, J. E., Mayes, M. T., Meyer, N., Johnson, C., Swarzenski, P. W., Cohen, A. S., & Russell, J. M. (2010). Late-twentieth-century warming in Lake Tanganyika unprecedented since AD 500. *Nature Geoscience*, 3(6), 422.
- Thompson, L. G., Mosley-Thompson, E., Davis, M. E., Lin, P. N., Henderson, K. A., Cole-Dai, J., & Liu, K. B. (1995). Late glacial stage and Holocene tropical ice core records from Huascarán, Peru. *Science*, 269(5220), 46-50.
- Thompson, L. G. (2000). Ice core evidence for climate change in the Tropics: implications for our future. *Quaternary Science Reviews*, 19(1-5), 19-35.
- Thompson, L. G., Mosley-Thompson, E., Davis, M. E., & Brecher, H. H. (2011). Tropical glaciers, recorders and indicators of climate change, are disappearing globally. *Annals of Glaciology*, 52(59), 23-34.
- Vuille, M., Francou, B., Wagnon, P., Juen, I., Kaser, G., Mark, B. G., & Bradley, R. S. (2008). Climate change and tropical Andean glaciers: Past, present and future. *Earth-science reviews*, 89(3-4), 79-96.
- Vuille, M., Burns, S. J., Taylor, B. L., Cruz, F. W., Bird, B. W., Abbott, M. B., ... & Novello, V. F. (2012). A review of the South American monsoon history as recorded in stable isotopic proxies over the past two millennia. *Climate of the Past*, 8(4), 1309-1321.

Supplementary Material

Sample processing and measurement

Quartz-bearing bedrock samples were collected by Dr. Meredith Kelly (Dartmouth College) at both the Quelccaya Ice Cap and Rwenzori Mountains. Quartz extraction was conducted at Boston College by crushing/grinding samples to suitable sizes (250-800 μm), and etching in weak hydrofluoric and nitric acid to remove all mineral phases but quartz (Kohl and Nishiizumi, 1991).

Beryllium was extracted at Tulane University in June 2017 following the beryllium isolation methods used by Lamont-Doherty Earth Observatory (<http://www.ldeo.columbia.edu/tcn/>). The method involves dissolving pure quartz in hydrofluoric acid and nitric acid, followed by extraction of beryllium via cation and anion column chemistry. Carbon was isolated following the methods of Lifton et al. (2001) and Pigati (2004) at Tulane University in June 2017, which involves combustion of quartz in a vacuum sealed furnace to release the trapped carbon, followed by oxidation of the carbon to create CO_2 , and finally reduction to pure carbon in the form of graphite. This approach has been shown to be successful in separating meteoric cosmogenic ^{14}C from *in situ* ^{14}C (Lifton et al. 2001). Lastly, $^{10}\text{Be}/^9\text{Be}$ ratios were measured in August 2017 at Lawrence Livermore Center for Accelerator Mass Spectrometry relative to the 07KNSTD3110 standard ratio of 2.85×10^{-12} (Nishiizumi et al., 2007) and $^{14}\text{C}/^{13}\text{C}$ ratios were measured at Woods Hole National Ocean Sciences Accelerator Mass Spectrometry facility, and used to calculate the concentrations of ^{10}Be and ^{14}C in the samples (Supplementary Table S1, S2, S3, S4).

Numerical Model

I developed a numerical model to simulate nuclide production, decay, and erosion for each sample to test possible glacier histories that would yield cosmogenic radionuclide concentrations and ratios in agreement with the measured values for each sample. The model creates a bedrock depth profile of ^{10}Be and ^{14}C concentrations through time given various glacier scenarios, driving production when exposed, and decay and erosion when ice covered. Production and decay rates are fixed, but erosion rates are systematically adjusted to explore a range of possibilities.

Surface production rates for each nuclide from spallation and muon reactions are taken from the CRONUS Earth Calculator v3 (Balco et al., 2008) using the LSD scaling model (Lifton et al., 2014). The surface production rates are then scaled with depth into bedrock via the attenuation length of each production pathway (Gosse and Phillips, 2001). The evolution of nuclide concentrations in a bedrock column are then driven by a prescribed exposure/erosion scenario in 100-year time steps via equation 1.

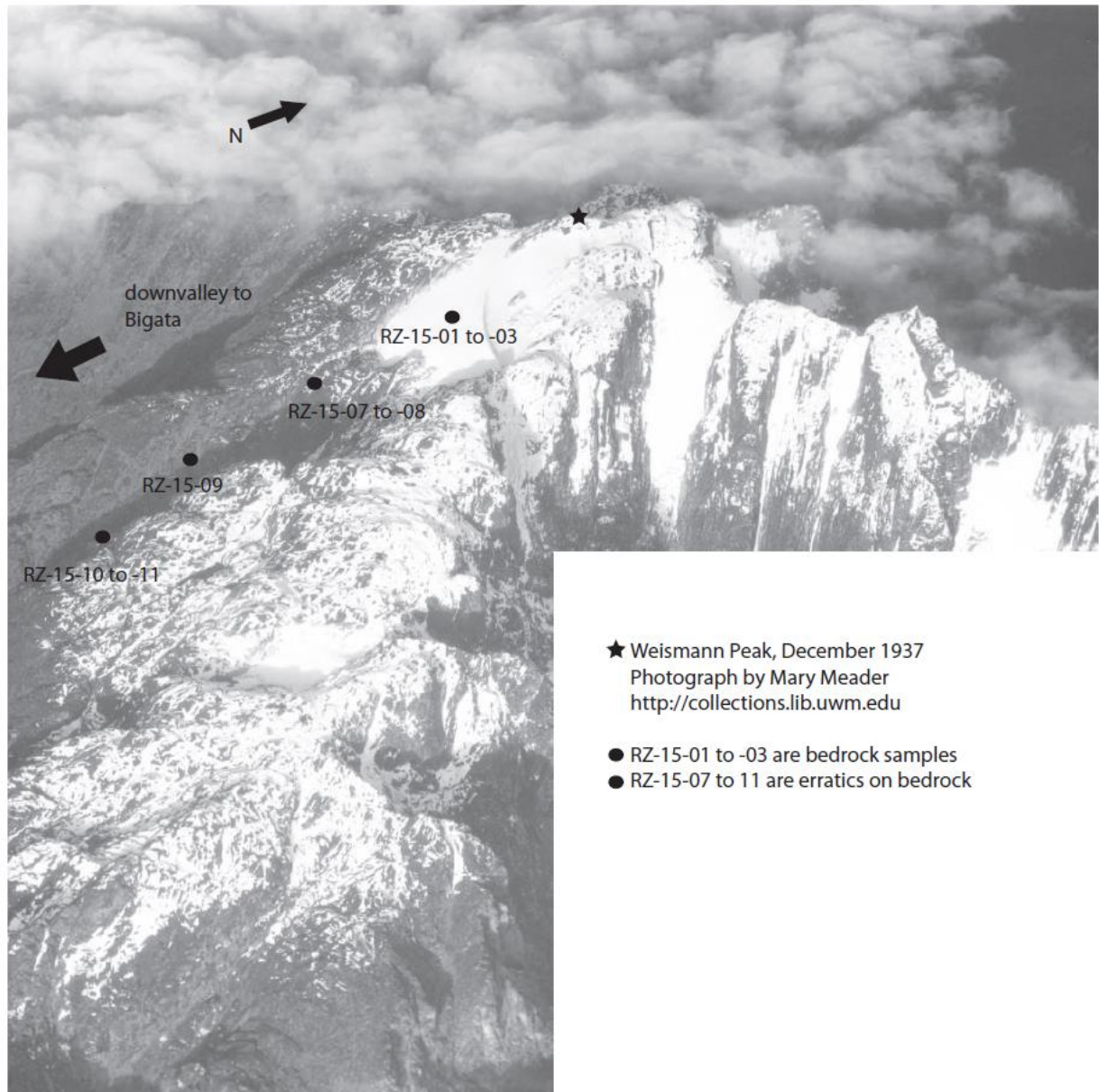
$$N(z, t) = P_{NT}(z) \cdot t + N(z, t - 1) \cdot e^{(-\lambda_N \cdot t)} \quad (1)$$

Where N is the concentration of the nuclide in the bedrock as a function of depth (z) and time (t), P_{NT} is the total production of the nuclide via spallation and muon production as a function of depth, and λ_N is the decay constant of the nuclide. During times of exposure, the model utilizes the production (P_{NT}) portion of equation 1. During times of burial, the model only utilizes the decay portion of equation 1 (right of the addition sign). Erosion is incorporated by redefining the “surface” as some depth below the top of the bedrock. The model assumes that erosion only takes place during times of burial. The 100-year time step was chosen because it offered a balance of resolution and computational simplicity.

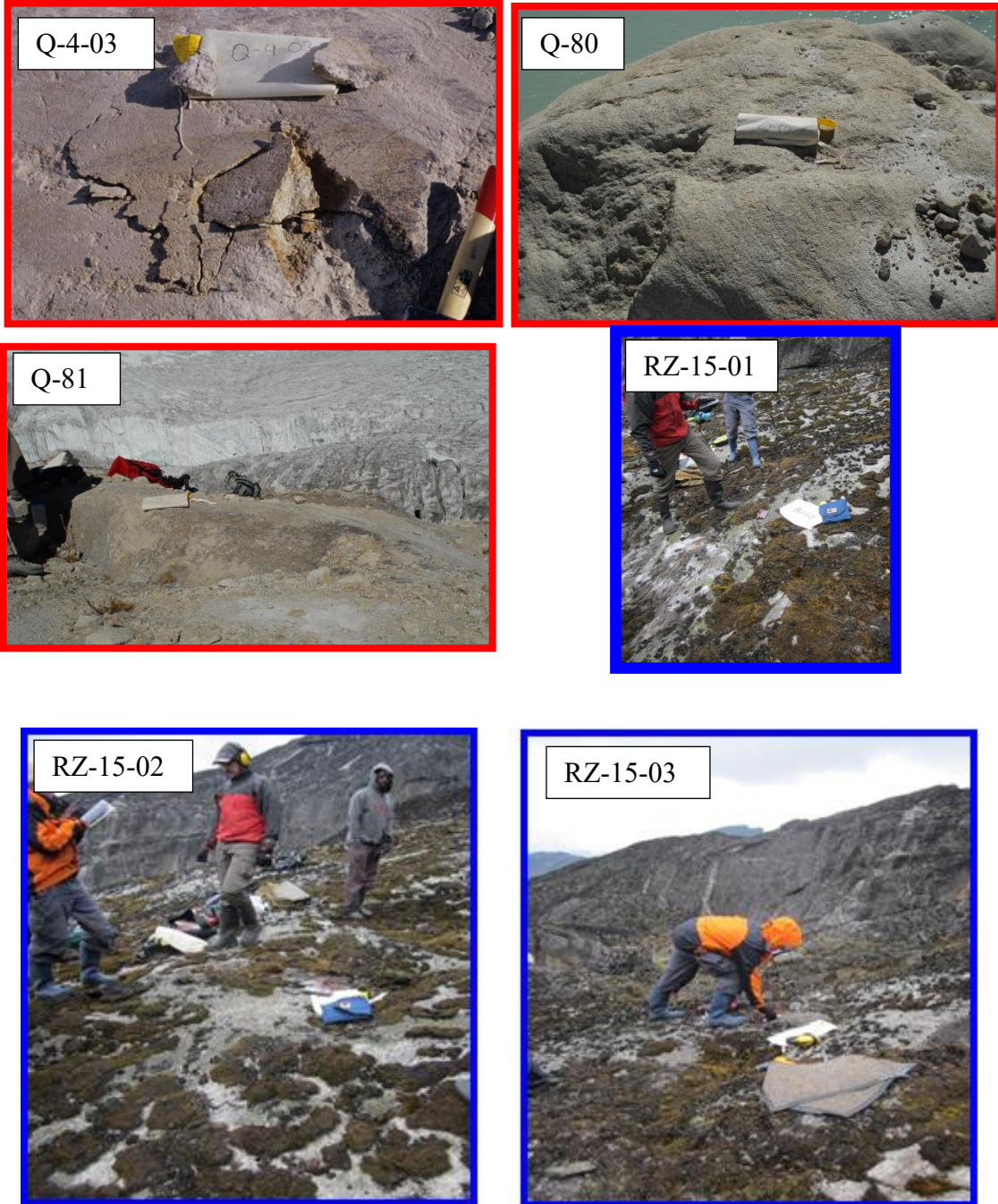
With larger time steps the simulation was too coarse and often either over or under predicted nuclide concentrations. Smaller time steps, on the other hand, made the computations much more laborious and thus were not time efficient.

100,000 exposure/burial scenarios were generated with the intent to sample a wide range of Holocene histories (Supplementary Figure S3). Twenty randomly sized blocks of exposure from 500 to 2000 years in length were randomly inserted into an 11.6 kyr year history of burial, and allowed to overlap. The total exposure ranges from 2 kyr to the full length of the history (11.6 kyr), with most scenarios between 5 to 8 kyr (Supplementary Figure S4). This distribution was chosen because the measured ^{10}Be concentrations suggest at least ~ 5 kyr of exposure, while the measured $^{14}\text{C}/^{10}\text{Be}$ ratios suggest at least several kyr of burial. The median ages of exposure (i.e., half of exposure happens before, half of exposure happens after) for the scenarios are distributed throughout the full range of possible histories (Supplementary Figure S5). The model tested erosion rates of 0 to 0.5 mm/yr (in steps of 0.01 mm/yr) for the Quelccaya Ice Cap samples and 0 to 0.03 mm/yr (in steps of 0.001 mm/yr) for the Rwenzori Mountain samples with each scenario. These ranges were selected based on several trial runs of the model.

Each sample was stepped through each exposure scenario (trying all erosion rates) individually, and the scenario was saved if the final surface ^{14}C and ^{10}Be concentrations was within 3σ uncertainty of the sample concentration, including both measurement and production rate (5% for ^{14}C and 7.9% for ^{10}Be , 1σ) uncertainties (Supplementary Figure S5). Scenarios that successfully simulate all samples are considered plausible Holocene histories.



Supplementary Figure S1. Aerial photo of Weismann Peak, Rwenzori Mountains, from 1937. Samples RZ-15-01 to -03 used for this study are shown to be covered by ice at the time the photo was taken. These samples have since been exposed and the peak is now ice free.



Supplementary Figure S2. Photographs of recently deglaciated bedrock samples from the Quelccaya Ice Cap (blue) and Rwenzori Mountains (red).

Supplementary Table S3. ^{10}Be and ^{14}C sample data. All uncertainties are 1σ .

Sample	Latitude (DD)	Longitude (DD)	Elevation (m asl)	Thickness (cm)	Shielding	$^{10}\text{Be}^1$ (10^4 atoms/g)	$^{14}\text{C}^1$ (10^4 atoms/g)	^{10}Be age ² (yr)	^{14}C age ² (yr)	$^{14}\text{C}/^{10}\text{Be}$
<i>Rwenzori Mountains</i>										
RZ-15-01	0.32793	29.88877	4509	1.9	0.969	16.57±0.18	13.77±0.54	5323±58	1701±74	0.83±0.03
RZ-15-02	0.32786	29.88887	4526	1.4	0.97	16.89±0.18	18.10±0.56	5346±58	2347±84	1.07±0.04
RZ-15-03	0.32781	29.88871	4536	2.8	0.97	18.89±0.17	17.97±0.56	5827±52	2347±85	0.95±0.03
<i>Quelccaya Ice Cap – ice marginal bedrock</i>										
Q-2-03	-13.9299	-70.8531	5225	3.0	0.969	25.62±0.57	21.60±0.78	5656±52	1959±80	0.84±0.04
Q-3-03	-13.93	-70.8526	5210	5.0	0.995	1.80±0.12	2.01±0.71	386±26	152±54	1.12±0.40
Q-4-03	-13.9298	-70.853	5220	4.0	0.995	21.69±0.43	26.20±0.84	4868±92	2464±92	1.21±0.05
Q-80	-13.9327	-70.8537	5196	3.0	0.996	12.08±0.28	13.40±0.76	2824±65	1113±68	1.11±0.07
Q-81	-13.9332	-70.8567	5225	3.0	0.997	56.00±1.34	19.80±0.79	10970±263	1720±76	0.35±0.02
<i>Quelccaya Ice Cap - down valley bedrock</i>										
Q-74	-13.909	-70.8747	5032	2.0	0.997	51.59±0.99	-	10920±210	-	-
Q-75	-13.909	-70.8747	5034	2.0	0.997	52.05±1.00	-	10975±211	-	-

¹Corrected for background ^{14}C and ^{10}Be . See Supplementary Table S3 and S4 for background measurements.

²Calculated using the CRONUS-Earth online calculator v.3 (Balco et al., 2008) with the LSDn scaling scheme (Lifton et al., 2014). Ages assume continuous exposure with no erosion. Uncertainties are analytical (i.e., internal) only.

Supplementary Table S4. ^{10}Be sample data details. Concentration of ^9Be carrier is 1040 ppm. All uncertainties are 1σ .

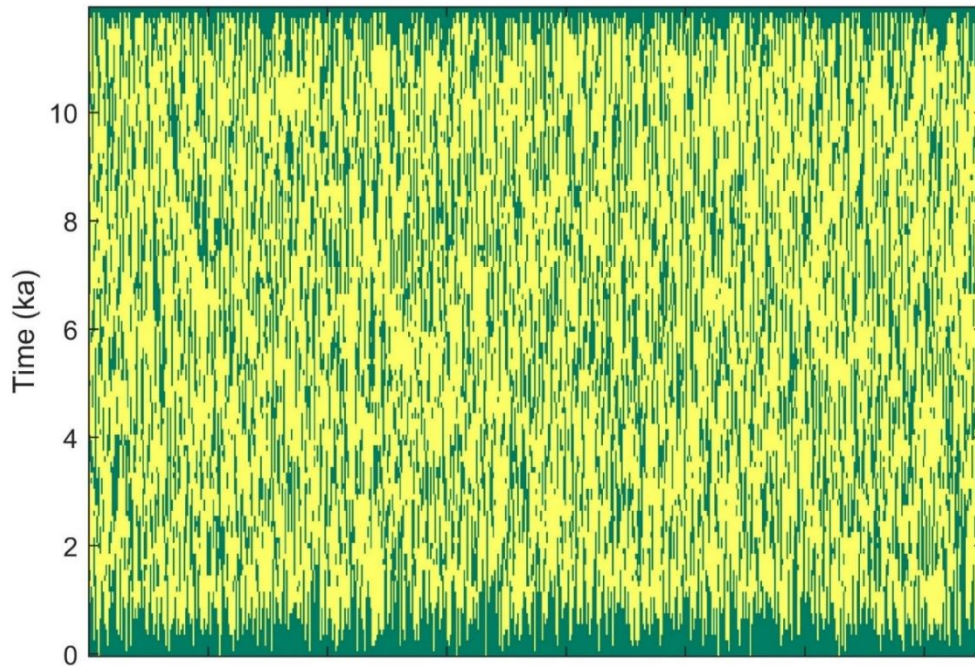
Sample	Be Carrier Added (g)	$^{10}\text{Be}/^9\text{Be}$ (10^{-13})	Quartz Mass (g)	^{10}Be Blank
<i>Rwenzori Mountains</i>				
RZ-15-01	0.1285	19.4±0.21	100.5702	MJ-BL65
RZ-15-02	0.1293	19.7±0.22	100.7899	MJ-BL65
RZ-15-03	0.1243	23.0±0.20	101.3296	MJ-BL65
<i>Quelccaya Ice Cap</i>				
Q-2-03	0.2601	2.92±0.05	20.0666	BAB_061517
Q-3-03	0.2601	0.28±0.01	20.0336	BAB_061517
Q-4-03	0.2601	2.24±0.04	18.0134	BAB_061517
Q-80	0.2601	1.44±0.03	20.3979	BAB_061517
Q-81	0.2607	6.27±0.13	20.0366	BAB_061517

Supplementary Table S3. ^{14}C sample data details. All uncertainties are 1σ .

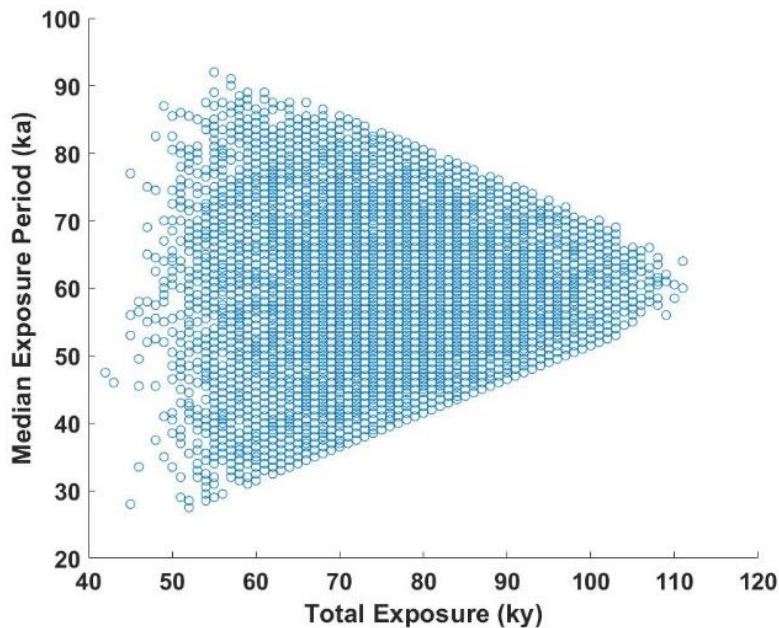
Sample ID	Quartz Mass (g)	C Yield (μg)	Diluted C Mass (μg)	$^{14}\text{C}/^{13}\text{C}$ (10^{-10}) *graphitization corrected	$\delta^{13}\text{C}$	$^{14}\text{C}/\text{C}$ (10^{-13})	Blank Corrected ^{14}C (10^5 atoms)	^{14}C (atoms/g)	Eff. Blank (atoms) (10^4)
<i>Rwenzori Mountains</i>									
RZ-15-01	5.0125	9.7 \pm 0.1	104.2 \pm 1.3	13.74 \pm 0.00009675	-4.56 \pm 2.52	10.507 \pm 0.00110	6.922 \pm 0.05947	138101 \pm 2336	9.533 \pm 0.5947
RZ-15-02	4.9938	11.5 \pm 0.1	103.9 \pm 1.3	17.49 \pm 0.00008598	-5.48 \pm 2.22	1.917 \pm 0.001003	9.036 \pm 0.05947	180936 \pm 2825	9.533 \pm 0.5947
RZ-15-03	5.0002	7.8 \pm 0.1	104.8 \pm 1.3	17.39 \pm 0.00008721	-5.21 \pm 2.72	1.907 \pm 0.001043	9.065 \pm 0.05947	181294 \pm 2828	9.533 \pm 0.5947
<i>Queccaya Ice Cap</i>									
Q-2-03	3.4872	5.5	104.5 \pm 1.3	14.74 \pm 0.0001008	9.64 \pm 2.31	1.641 \pm 0.001162	7.643 \pm 0.05947	219162 \pm 3588	9.533 \pm 0.5947
Q-3-03	3.7742	5.0	111.3 \pm 1.4	30.83 \pm 0.0000072	11.49 \pm 2.05	0.3437 \pm 0.0003476	0.9645 \pm 0.05947	25555 \pm 1705	9.533 \pm 0.5947
Q-4-03	3.5279	9.1	111.1	16.740 \pm 0.0001031	10.92 \pm 2.32	1.865 \pm 0.001199	0.9436 \pm 0.05947	267461 \pm 4131	9.533 \pm 0.5947
Q-80	3.4983	6.3	107.3	969.8 \pm 0.00005272	9.18 \pm 1.92	1.079 \pm 0.0006096	0.4849 \pm 0.05947	138623 \pm 2721	9.533 \pm 0.5947
Q-81	3.5603	5.3	108.4	13.48 \pm 0.00006420	11.16 \pm 2.47	1.503 \pm 0.000741	0.7214 \pm 0.05947	202616 \pm 3379	9.533 \pm 0.5947

Supplementary Table S4. ^{10}Be blank data. Concentration of ^9Be carrier is 1040 ppm. Uncertainties are 1σ .

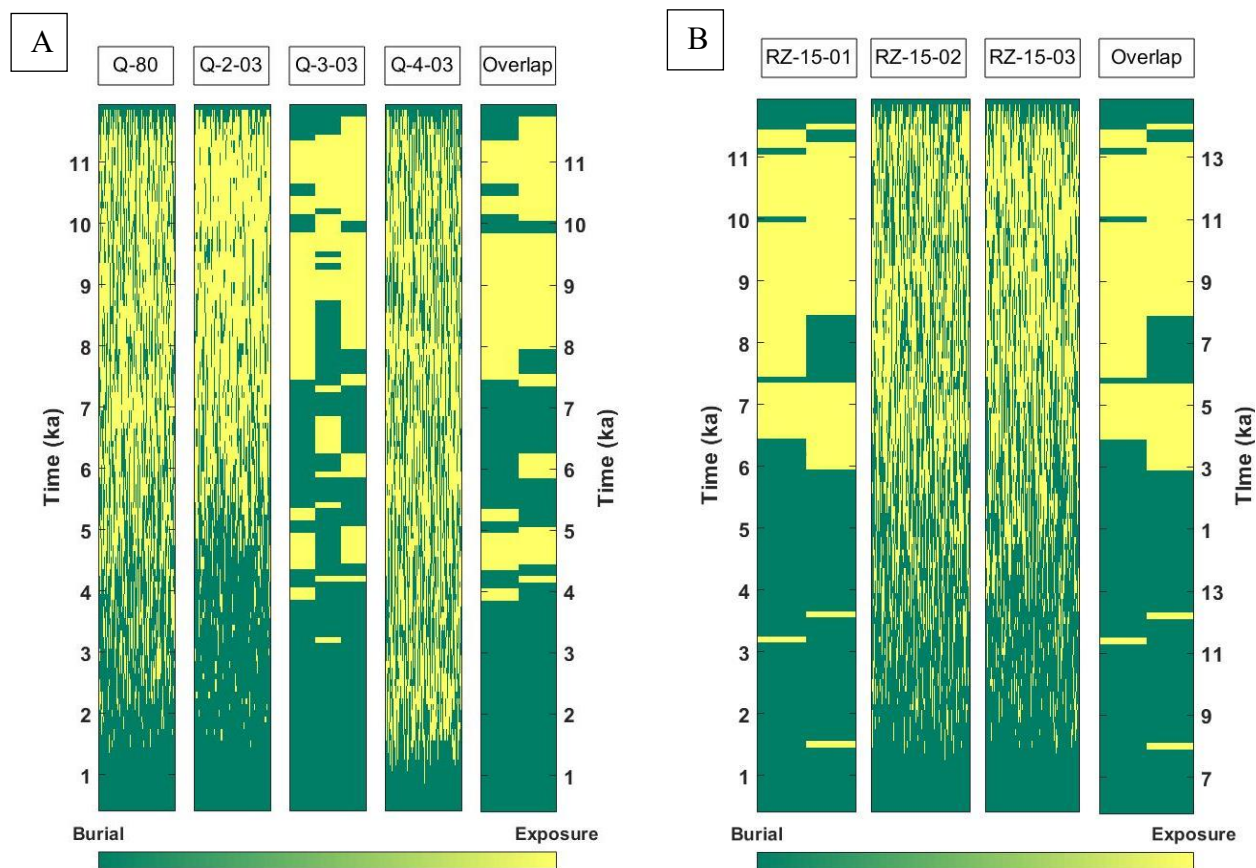
Blank ID	Be carrier (g)	$^{10}\text{Be}/^9\text{Be}$ (10^{-15})	^{10}Be (10^4 atoms)
BAB_061517	0.2585	8.10 \pm 0.76	14.56 \pm 1.36
MJ-BL65	0.01285	7.00 \pm 0.58	0.6251 \pm 0.0518



Supplementary Figure S3. Graphical depiction of all modeled Holocene exposure scenarios (n=100,000). Yellow indicates periods of exposure (glacier is smaller than today), green indicates periods of burial (glacier is larger than today). Each vertical line represents a single scenario.

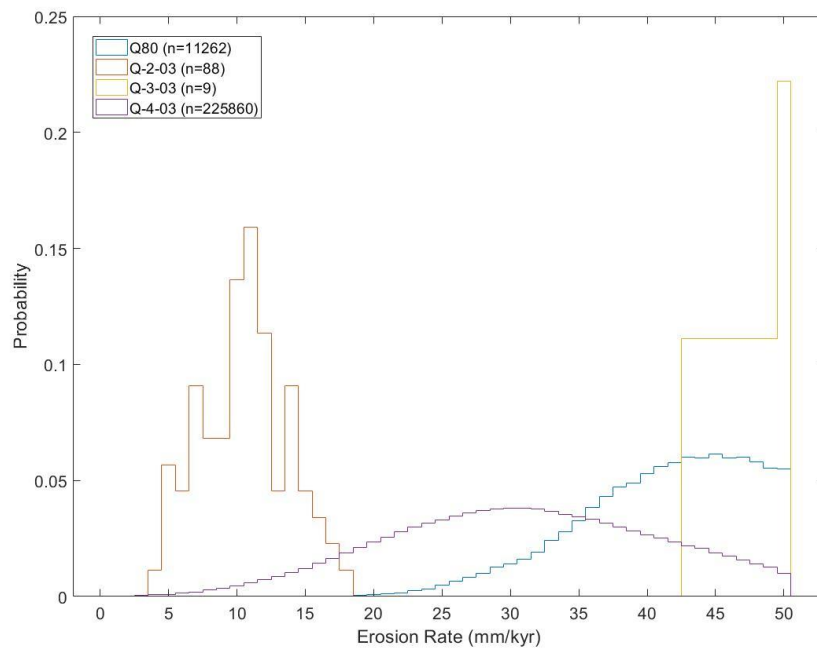


Supplementary Figure S4. The median age of exposure and cumulative exposure duration for each modeled exposure scenario. Each point is one scenario. The distribution shows a wide spread in the timing and duration of exposure, which allows the model to thoroughly explore Holocene scenarios consistent with the measured data

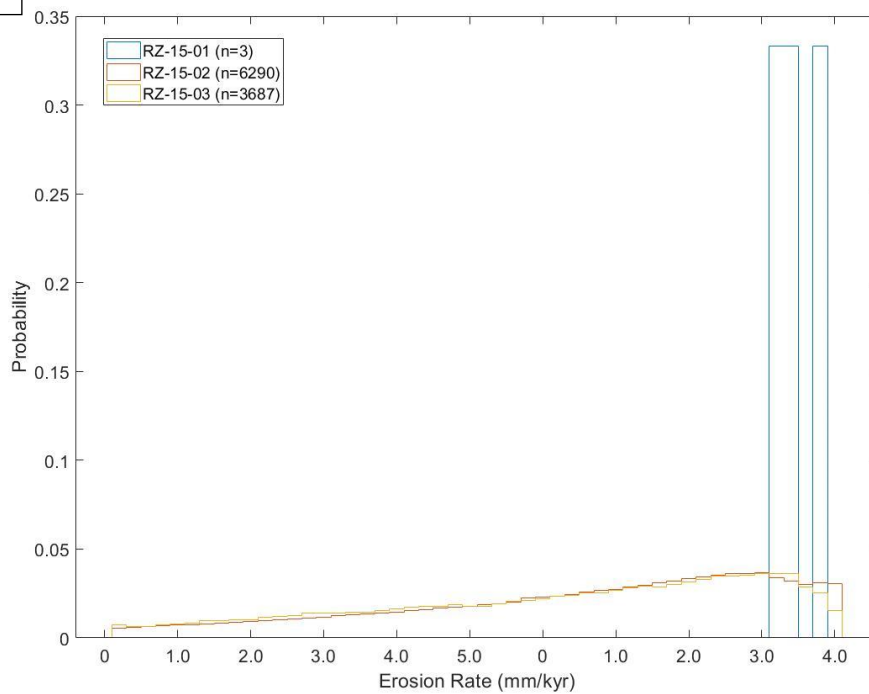


Supplementary Figure S5. Exposure scenarios that yield ^{14}C and ^{10}B concentrations within 3σ of the measured samples for the **A)** Quelccaya Ice Cap and **B)** Rwenzori Mountains samples. Yellow indicates periods of exposure (glacier is smaller than today), green indicates periods of burial (glacier is larger than today). Each vertical line is a separate scenario. Panels show scenarios consistent with each sample individually (labeled above each panel) as well as all of the samples (“Overlap”).

A



B



Supplementary Figure S6: Simulated erosion rates for successful model scenarios for the **A)** Quelccaya Ice Cap and **B)** Rwenzori Mountains samples. Frequency of erosion rates is represented as probability for scaling purposes. Total counts for each sample given in legend.

Supplemental References

- Balco, G., Stone, J. O., Lifton, N. A., & Dunai, T. J. (2008). A complete and easily accessible means of calculating surface exposure ages or erosion rates from ^{10}Be and ^{26}Al measurements. *Quaternary geochronology*, 3(3), 174-195.
- Buffen, Aron M., et al. (2009). "Recently exposed vegetation reveals Holocene changes in the extent of the Quelccaya Ice Cap, Peru." *Quaternary Research* 72.2: 157-163.
- Gosse, John C., and Fred M. Phillips. "Terrestrial in situ cosmogenic nuclides: theory and application." *Quaternary Science Reviews* 20.14 (2001): 1475-1560.
- Kohl, C. P., & Nishiizumi, K. (1992). Chemical isolation of quartz for measurement of in-situ-produced cosmogenic nuclides. *Geochimica et Cosmochimica Acta*, 56(9), 3583-3587.
- Lifton, N. A., Jull, A. T., & Quade, J. (2001). A new extraction technique and production rate estimate for in situ cosmogenic ^{14}C in quartz. *Geochimica et Cosmochimica Acta*, 65(12), 1953-1969.
- Lifton, N., Sato, T., & Dunai, T. J. (2014). Scaling in situ cosmogenic nuclide production rates using analytical approximations to atmospheric cosmic-ray fluxes. *Earth and Planetary Science Letters*, 386, 149-160.
- Nishiizumi, K., Imamura, M., Caffee, M. W., Southon, J. R., Finkel, R. C., & McAninch, J. (2007). Absolute calibration of ^{10}Be AMS standards. *Nuclear Instruments and Methods in Physics Research Section B: Beam Interactions with Materials and Atoms*, 258(2), 403-413.
- Pigati, Jeffrey S., and Nathaniel A. Lifton. "Geomagnetic effects on time-integrated cosmogenic nuclide production with emphasis on in situ ^{14}C and ^{10}Be ." *Earth and Planetary Science Letters* 226.1-2 (2004): 193-205.

MATLAB model code for Quelccaya Ice Cap

Note: The Rwenzori Mountains model is the same, except that it simulated a smaller and finer range (sub-millimeter) of erosion rates, which required a few additional lines of code in the depth profile interpolation section.

```
savename=input('What do you want to name the save file? (name.mat)','s'); % Save your outputs  
for later analysis (make sure you put .mat at the end of the name you choose)
```

```
%% This section clears out variables from previous runs that may cause problems in the current  
run (read if you are trying to repeat a previous run)
```

```
close all %close all open figures
```

```
clear ec %clear the previous scenarios (if you are conducting a fresh run. If you want to re-use  
scenarios from a previous run make sure to block out this line)
```

```
clear ers %clear erosions from previous runs
```

```
clear hit_barcodes %clear the hits from previous runs
```

```
clear hit_er %clear the hit erosions from the previous runs
```

```
clear hit %clear the hit index from previous runs
```

```
clear P10 %clear the Be production rates from previous runs (in case you are adding or removing  
samples from a run)
```

```
clear P14 %clear the C production rates from previous runs
```

```
clear totalexp %clear the total exposure variable from previous runs
```

```
clear med %clear the median exposure value from previous runs
```

```

clear m %clear the mean exposure value from previous runs

clear s %clear the standard deviation of exposure from previous runs

load 'QIC_7_25.mat' %load a previous trial (block out if doing fresh run)

%% This section is for inputting the sample specific information

% Must be a txt file in the format used for the Cronus Earth Calculator V4

%sample name lat long elv std thickness density shielding factor 14C conc 14C err 10Be conc
10Be err standard uplift curve

% example:

% Q-80 -13.9327 -70.8537 5196 std 3 2.65 0.996 0 138623.49 2720.78
120789.0327 2775.04113 07KNSTD none

file = input('Please enter the name of the sample data file','s'); % input txt file name

FID = fopen(file); %opens txt file

data = textscan(FID,'%s %n %n %n %s %n %n %n %n %n %n %n %n %s %s'); %reads in txt
file

fclose(FID); %closes txt file

dstring="";

%makes variables for the samples from the information in the txt file

all_sample_name = data{1}; %sample name

all_lat = data{2}; % latitude

```

```
all_long = data{3}; % longitude
all_elv = data{4}; %elevation
all_pressure = data{4}; %pressure
all_aa = data{5}; % pressure identifier
all_thick = data{6}; %thickness
all_rho = data{7}; %density
all_shielding = data{8}; %shielidng
all_E = data{9}; %
all_N14 = data{10}; %14C Conc.
all_delN14 = data{11}; %14C conc err
all_N10 = data{12}; %10Be conc
all_delN10 = data{13}; %10Be conc err
all_be_std_name = data{14}; %10Be standard name
all_curve = data{15}; %uplift curve
```

```
%% This section sets up the variables used in the model
```

```
To=11600; %input length of time you want model to run (years)
```

```
Ts=100; %input time step you want to run (if your runs are taking a while consider changing to a  
coarser time step) (years)
```

```
scennum=100000; %number of scenarios
```

```
load Q_Depth.mat %load Depth profile for QIC (Provided by Brent Goehring)
```

```

%prior versions generated Depth Profiles using the MATLAB cronus earth
%calculator (contact anthonycolevickers@gmail.com if you wish to do that)

N10n=all_N10/Q.Q_2_03.P10_tot(1,1); %production rate normalized 10Be conc.
N14n=all_N14/Q.Q_2_03.P14_tot(1,1); %production rate normalized 14C conc.
delN10n=sqrt(((all_delN10./all_N10).^2)+(.079^2)).*N10n; %1 sigma error from conc.
uncertainty and production rate uncertainty for 10Be
delN14n=sqrt(((all_delN14./all_N14).^2+(0.019^2)).*N14n;%1 sigma error from conc.
uncertainty and production rate uncertainty for 14C

PR10(:,1)=Q.Q_2_03.P10_tot./Q.Q_2_03.P10_tot(1,1); %Normalized production rate profile for
10Be (normalized to surface production rate)
PR14(:,1)=Q.Q_2_03.P14_tot./Q.Q_2_03.P14_tot(1,1);%Normalized production rate profile for
14C (normalized to surface production rate)

e=Q.Q_2_03.z; %depth of profile in cm

%interpolating each production profile from each sample into mm (from
%g/cm2)

p10(1:length(PR10),1) = PR10(:,1); %10Be depth profile in cm steps
p14(1:length(PR10),1) = PR14(:,1); %14C depth profile in cm steps
x=e;

```

```

xq=0:1/10:501;

P10(1:length(xq),1)=interp1(x,p10(:,1),xq); %interpolating the depth profile into mm
P14(1:length(xq),1)=interp1(x,p14(:,1),xq); %interpolating the depth profile into mm

%% This section generates random exposure/burial scenarios given a number of scenarios
desired and the total length of history desired

%where 1=exposure and 0=burial.

i=1; %initialize counter

while i<=scennum %produce scenarios until i equals the number of scenarios

s=randi(9,20,1); % randomize size of blocks

p=randi(((To/Ts)-12),20,1); % randomize position of blocks

e1=ones(s(1),1); %block 1 (made of 1's to denote exposure)
e2=ones(s(2),1); %block 2
e3=ones(s(3),1); %block 3...etc
e4=ones(s(4),1);
e5=ones(s(5),1);
e6=ones(s(6),1);
e7=ones(s(7),1);
e8=ones(s(8),1);
e9=ones(s(9),1);

```

```
e10=ones(s(10),1);
```

```
e11=ones(s(11),1);
```

```
e12=ones(s(12),1);
```

```
e13=ones(s(13),1);
```

```
e14=ones(s(14),1);
```

```
e15=ones(s(15),1);
```

```
e16=ones(s(16),1);
```

```
e17=ones(s(17),1);
```

```
e18=ones(s(18),1);
```

```
e19=ones(s(19),1);
```

```
e20=ones(s(20),1);
```

```
c=zeros((To/Ts),1); %make a variable of length Total time/ timestep to fill with the exposure  
blocks (1's)
```

```
c(p(1)+1:length(e1)+p(1))=e1; %insert block 1 into random position
```

```
c(p(2)+1:length(e2)+p(2))=e2;
```

```
c(p(3)+1:length(e3)+p(3))=e3;
```

```
c(p(4)+1:length(e4)+p(4))=e4;
```

```
c(p(5)+1:length(e5)+p(5))=e5;
```

```
c(p(6)+1:length(e6)+p(6))=e6;
```

```
c(p(7)+1:length(e7)+p(7))=e7;
```

```
c(p(8)+1:length(e8)+p(8))=e8;
```

```
c(p(9)+1:length(e9)+p(9))=e9;
```

```

c(p(10)+1:length(e10)+p(10))=e10;
c(p(11)+1:length(e11)+p(11))=e11;
c(p(12)+1:length(e12)+p(12))=e12;
c(p(13)+1:length(e13)+p(13))=e13;
c(p(14)+1:length(e14)+p(14))=e14;
c(p(15)+1:length(e15)+p(15))=e15;
c(p(16)+1:length(e16)+p(16))=e16;
c(p(17)+1:length(e17)+p(17))=e17;
c(p(18)+1:length(e18)+p(18))=e18;
c(p(19)+1:length(e19)+p(19))=e19;
c(p(20)+1:length(e20)+p(20))=e20;

```

```

ec(:,i)=c; %place generated scenario of 1's and 0's into ec (the scenario variable used in the
model) in column i
med(i)=median(find(ec(:,i))); %calculate the median position of exposure in the scenario
m(i)=mean(find(ec(:,i))); %calculate the mean position of the exposure in the scenario
s(i)=std(find(ec(:,i))); %calculate the standard deviation of the position of the exposure in the
scenario
i=i+1; %add 1 to the counter

end

```

```

%% This section generates figures for the scenarios

```

```
%total exposure history figure
```

```
figure
```

```
imagesc(ec);
```

```
totalexp=sum(ec);
```

```
figure
```

```
hist(totalexp);
```

```
xlabel('Total Exposure History (ky)')
```

```
ylabel('Frequency')
```

```
%gradient of the total exposure history (easier to visualize and
```

```
%understand)
```

```
grad=sum(ec,2);
```

```
figure
```

```
imagesc(grad);
```

```
figure
```

```
hist(grad)
```

```
%scatter plot of the median age of exposure
```

```
figure
```

```
scatter(totalexp,med)
```

```
xlabel('Total Exposure (ky)')
```

```
ylabel('Median Exposure Period (ka)')
```

```
%scatter plot of the total duration of exposure
```

```
figure
```

```
scatter(totalexp,m);
```

```
xlabel('Total Exposure (ky)')
```

```
ylabel('Mean Exposure Period (ka)')
```

```
%scatter plot of the standard deviation of the exposure position. (The spread of where the  
exposure is located within the total history)
```

```
figure
```

```
scatter(totalexp,s);
```

```
%% This section is the model that steps a bedrock profile through time given the exposure and  
burial history produced above
```

```
%The bedrock starts out with no nuclides. When exposed (1) the bedrock increase
```

```
%each nuclide at the normalized production rate (with decay factored in).
```

```
%When buried (0) the nuclides decrease at their decay rate.
```

```
%erosion occurs during burial. This is done by removing n amount of surface
```

```
%from the bedrock profile and using the new surface for further burial or
```

```
%production.
```

```
%the final modeled surface concentrations are compared to the measured
```

```

%concentrations. If the modeled concentration is within 3 sigma of the
%measured concentration the scenario is assigned a 1 in the hit variable
%which stores the outcomes of each tested scenario. If the modeled
%concentration is outside 3 sigma of the measured concentration it is labeled
%a 0 in the hit variable

tic % start a timer of progress

bedrock_10Be = zeros(10000,1); %initialize a bedrock profile for 10Be with no nuclides present
bedrock_14C = zeros(10000,1); %initialize a bedrock profile for 14C with no nuclides present

iter=size(ec,2); %number of scenarios

z = [1:3000]'; % depth range (3 meters) for modeled bedrock profile. Increase if you have
significant erosion as you might exhume very deep bedrock which is initialized at zero.

ers=unique(floor(linspace(0,50,50))); %create a vector of erosions (0 to 50 mm per 100 years)
ersidx= repmat(ers,[1,1,length(all_N10)]); %erosion index

hit=NaN(size(ec,2),length(ers),length(all_N10)); % create a vector of NaNs to store the hits.
(logical array)

for ii=1:size(ec,2) %for the number of scenarios (walk through the scenarios 1 at a time
fprintf('Processing %d of %d...!',ii,iter) %this is for letting you know the progress

for g=1:length(ers) %for the number of erosion amounts (walk through the erosion rates 1 at a
time)

```

```
for t=100:Ts:To %time from 100 to To at timestep Ts (walk through time from beginning of
total history to present at To timestep)
```

```
d(t/Ts)=ec(t/Ts,ii); %Use scenario ii at time t/Ts
```

```
if d(t/Ts)==1 % if the scenario at time t/Ts is exposure
```

```
bedrock_10Be(1:length(z),t/Ts+1) = 1*P10(1+0:length(z)+0,1)*Ts+
(bedrock_10Be(1+0:length(z)+0,(t/Ts))*exp(-1*4.99e-7*Ts)); %increase the 10Be bedrock
concentration (production - decay)
```

```
bedrock_14C(1:length(z),t/Ts+1) = 1*P14(1+0:length(z)+0,1)*Ts +
(bedrock_14C(1+0:length(z)+0,(t/Ts))*exp(-1*0.00012096809*Ts)); %increase the 14C bedrock
concentration
```

```
elseif d(t/Ts)==0 %if the scenario at time t/Ts is burial
```

```
er=ers(g); %erosion in mm/timestep. need to make sure this makes sense for your
timeframe.
```

```
bedrock_10Be(1:length(z),t/Ts+1) = 0*P10(1+er:length(z)+er,1)*Ts+
(bedrock_10Be(1+er:length(z)+er,(t/Ts))*exp(-1*4.99e-7*Ts)); %decrease the 10Be bedrock
concentration by erosion and decay
```

```
bedrock_14C(1:length(z),t/Ts+1) = 0*P14(1+er:length(z)+er,1)*Ts +
(bedrock_14C(1+er:length(z)+er,(t/Ts))*exp(-1*0.00012096809*Ts)); %decrease the 14C
bedrock concentration by erosion and decay
```

```
end
```

end

```
hit(ii,g,:)= bedrock_10Be(1,end)<(N10n+(3*delN10n)) & (bedrock_10Be(1,end))>(N10n-  
(3*delN10n)) &...
```

```
(bedrock_14C(1,end)<(N14n+(3*delN14n))& (bedrock_14C(1,end))>(N14n-  
(3*delN14n)); %for the scenario number and erosion rate, if the final surface concentration is  
within 3 sigma of the 10Be and 14C concentration put a 1 in the hit variable. Otherwise put a 0.  
(logical statment)
```

end

```
fprintf('done.\n')
```

end

```
toc %end timer
```

```
save(savename) %save the output
```

```
%% This section compares the hits from each sample and locates scenarios that were hits for all  
samples
```

```
[r1,c1]=find(hit(:,1)); %find the row (scenario number) and column (erosion rate) that were hits  
in sample 1...etc.
```

```
[r2,c2]=find(hit(:,:,2));
```

```
[r3,c3]=find(hit(:,:,3));
```

```
[r4,c4]=find(hit(:,:,4));
```

```
[r5,c5]=find(hit(:,:,5));
```

```
%generate a variable of the index numbers of hit scenarios that appeared in
```

```
%all samples
```

```
%note: there may be some samples that have no hits, or some that have no
```

```
%hits in common with other samples. You may need to do some cross
```

```
%comparisons or modify the script to analyze only the samples that probably
```

```
%have similar scenarios
```

```
scen_matchidx=r1(ismember(r1,r2));
```

```
scen_matchidx=scen_matchidx(ismember(scen_matchidx,r3));
```

```
scen_matchidx=scen_matchidx(ismember(scen_matchidx,r4));
```

```
scen_matchidx=scen_matchidx(ismember(scen_matchidx,r5));
```

```
scen_match=ec(:,scen_matchidx); %make a variable of hit scenarios that were common for all  
samples (index the full scenario array)
```

```
hit_barcodes_sum=sum(scen_match,2,'omitnan'); %sum up the total exposure for each scenario
```

```
%% figures: Plots the hit scenarios
```

```

time=-((To/Ts)/10):1];
tick=[0:10:150];
figure
colormap(jet)
imagesc(scen_match)
% set(gca, 'XTick', [1:length(hit_er)], 'XTickLabel', hit_er)
% xlabel('Erosion (mm/100 years)')
set(gca,'ytick',tick)
ylabel('time (ka)')
yticklabels({time});

figure(3)
colormap(jet)
imagesc(hit_barcodes_sum)
ylabel('time (12 ka=0, 115=present)')
set(gca,'ytick',tick)
ylabel('time (ka)')
yticklabels({time});

```